# A Novel Antiferromagnetic Organic Superconductor $\kappa$-$(BETS)_2FeBr_4$ [Where BETS = Bis(ethylenedithio)tetraselenafulvalene]

**Hideki Fujiwara,[†] Emiko Fujiwara,[†,§] Yasuhiro Nakazawa,[†] Bakhyt Zh. Narymbetov,[†] Kiyonori Kato,[†] Hayao Kobayashi,*[,†] Akiko Kobayashi,[‡] Madoka Tokumoto,[§,†] and Patrick Cassoux[⊥]**

*Contribution from the Institute for Molecular Science, Myodaiji, Okazaki 444-8585, Japan, Research Centre for Spectrochemistry, Graduate School of Science, The University of Tokyo, Hongo, Bunkyo-ku, Tokyo 113-0033, Japan, Electrotechnical Laboratory, Umezono, Tsukuba 305-0045, Japan, and Equipe Précurseurs Moléculaires et Matériaux, LCC-CNRS, 205 Route de Narbonne, 31077 Toulouse Cedex 04, France*

*Received July 5, 2000*

**Abstract:** The electrical and magnetic properties of $\kappa$-$(BETS)_2FeBr_4$ salt [where BETS = bis(ethylenedithio)-tetraselenafulvalene] showed that this system is the first antiferromagnetic organic metal at ambient pressure ($T_N$ = 2.5 K). The characteristic field dependence of the magnetization at 2.0 K indicates a clear metamagnetic behavior. The small resistivity drop observed at $T_N$ clearly shows the existence of the interaction between $\pi$ metal electrons and localized magnetic moments of $Fe^{3+}$ ions. In addition, this system underwent a superconducting transition at 1.1 K. That is, $\kappa$-$(BETS)_2FeBr_4$ is the first antiferromagnetic organic metal exhibiting a superconducting transition below Néel temperature. The magnetic field dependence of the superconducting critical temperature indicated that the superconductivity in this system is strongly anisotropic also in the conduction plane because of the existence of the metamagnetically induced internal field based on the antiferromagnetic ordering of the $Fe^{3+}$ 3d spins in contrast to the cases of the other conventional organic superconductors. Furthermore, the specific heat measurement exhibited a $\lambda$-type large peak of zero-field specific heat corresponding to the three-dimensional antiferromagnetic ordering of high-spin $Fe^{3+}$ ions. The lack of distinct anomaly in the $C_p$ vs $T$ curve at $T_c$ suggests the coexistence of the superconductivity and the antiferromagnetic order below $T_c$.

## Introduction

The chemistry and physics of organic conductors has made great strides since the discovery of the first one-dimensional organic metal, tetrathiafulvalene−tetracyano-*p*-quinodimethane (TTF·TCNQ) complex, in 1973.[1,2] The designability of organic systems has encouraged many chemists to produce completely new types of conducting systems. In contrast to the complicated molecular and crystal structures of organic conductors, their electronic structures are surprisingly simple and the investigations on Shubnikov−de Haas and de Haas−van Alphen oscillations have elucidated their simple Fermi surfaces. Among the TTF derivatives synthesized so far, bis(ethylenedithio)-TTF (BEDT-TTF) has played the most important role in the development of organic conductors and has yielded many organic superconductors so far such as $\kappa$-type BEDT-TTF

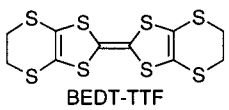


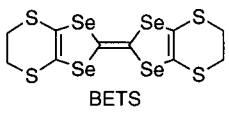


superconductors, where transverse intermolecular S−S networks play an essential role in forming a two-dimensional Fermi surface.[3−6] In the recent studies of molecular conductors, one of the most exciting topics is the development of the hybrid systems consisting of organic donor molecules and inorganic magnetic anions such as the paramagnetic organic superconductor $\beta''$-$(BEDT\text{-}TTF)_4(H_2O)Fe(C_2O_4)_3(C_6H_5CN)$, in which the

[†] Institute for Molecular Science.
[§] Electrotechnical Laboratory.
[‡] The University of Tokyo.
[⊥] Equipe Précurseurs Moléculaires et Matériaux.

(1) Ferraris, J.; Cowan, D. O.; Walatka, V., Jr.; Perlstein, J. H. *J. Am. Chem. Soc.* **1973**, *95*, 948−949.

(2) Recent Proceedings of the International Conferences: (a) Proceedings of the International Conference on Science and Technology of Synthetic Metals, Snowbird: Vardeny, Z. V.; Epstein, A. J., Eds. *Synth. Met.* **1997**, *84*−*86*. (b) Proceedings of the International Conference on Science and Technology of Synthetic Metals, Montpellier: Bernier, P.; Lefrant, S.; Bidan, G., Eds. *Synth. Met.* **1999**, *101*−*103*. (c) Proceedings of the Symposium on Advances in the Chemistry and Physics of Novel Low-Dimensional and Conducting or Superconducting Solids, Honolulu: Williams, J. M.; Geiser, U.; Mori, T.; Eldridge, J. E., Eds. *Mol. Cryst. Liq. Cryst.* **1996**, *284*.

(3) Kobayashi, A.; Kato, R.; Kobayashi, H.; Moriyama, S.; Nishio, Y.; Kajita, K.; Sasaki, W. *Chem. Lett.* **1987**, 459−462.

(4) (a) Williams, J. M.; Ferraro, J. R.; Thorn, R. J.; Carlson, K. D.; Geiser, U.; Wang, H. H.; Kini, A. M.; Whangbo, M.-H. *Organic Superconductors*; Prentice Hall: Englewood Cliffs, NJ, 1992. (b) Ishiguro T.; Yamaji, K.; Saito, G. *Organic Superconductors*, 2nd ed.; Springer-Verlag: Berlin, Heidelberg, 1998.

(5) Reviews: (a) Williams, J. M.; Schultz, A. J.; Geiser, U.; Carlson, K. D.; Kini, A. M.; Wang, H. H.; Kwok, W. K.; Whangbo, M.-H.; Schirber, J. E. *Science* **1991**, *252*, 1501−1508. (b) Saito, G. *Phosphorus, Sulfur, Silicon* **1992**, *67*, 345−360.

(6) (a) Parkin, S. S. P.; Engler, E. M.; Schumaker, R. R.; Lagier, R.; Lee, V. Y.; Scott, J. C.; Greene, R. L. *Phys. Rev. Lett.* **1983**, *50*, 270−273. (b) Yagubskii, E. B.; Schegolev, I. F.; Laukhin, V. N.; Kononovich, P. A.; Karatsovnik, M. V.; Zvarykina, A. V.; Buravov, L. I. *Pis'ma Zh. Eksp. Teor. Fiz.* **1984**, *39*, 12−15; *JETP Lett. (Engl. Transl.)* **1984**, *39*, 12−16.

10.1021/ja002439x CCC: $20.00 
Published on Web 12/16/2000

interaction between $\pi$ metal electrons of the donor molecules and localized magnetic moments of the anions has received much attention in creating new types of conducting systems.[7,8] The largest target among these systems may be an antiferromagnetic or ferromagnetic organic superconductor. We have investigated BETS salts involving transition metal halides such as $\lambda$-$(BETS)_2MCl_4$ [BETS = bis(ethylenedithio)tetraselenafulvalene; M = Ga and Fe] with a superconducting (M = Ga) or insulating (M = Fe) ground state.[9] Furthermore, we have recently found an exotic organic conductor, $\lambda$-$(BETS)_2Fe_xGa_{1-x}Br_yCl_{4-y}$ ($0 < x < 1$, $0 < y < 0.5$) exhibiting a superconductor-to-insulator or superconductor-to-metal transition. In these systems, the strong $\pi-d$ coupling between the $\pi$-metal electron systems of the BETS molecules and the localized $Fe^{3+}$ magnetic moments of the anions plays an important role in breaking the superconducting state of these systems and causes cooperatively an antiferromagnetic insulating state.[10] Contrary to the $\lambda$-type $(BETS)_2MCl_4$ system, the other main modifications, $\kappa$-$(BETS)_2MX_4$ (M = Ga, Fe, and In; X = Br and Cl), retain their metallic states down to 2 K.[9b,11] A crystal structure and an extended Hückel tight-binding band calculation suggest $\kappa$-$(BETS)_2FeCl_4$ to be a two-dimensional metal, which is consistent with recent low-temperature magnetoresistance experiments.[12] However, the ground states of $\kappa$-$(BETS)_2FeBr_4$ at the lowest temperature region remained unclear. In this paper, we report structures, magnetic, and electrical properties of an antiferromagnetic organic metal, $\kappa$-$(BETS)_2FeBr_4$.[13] We also investigated a magnetic field dependence of the electrical resistivities and its anisotropy. Furthermore, we also present a study on a specific heat measurement to clear the coexistence of the antiferromagnetic spin ordering and superconductivity.

## Results and Discussion

**Crystal and Band Structure Determination of $\kappa$-$(BETS)_2FeBr_4$.** Plate-shaped crystals were prepared electrochemically from a 10% ethanol−chlorobenzene solution containing BETS and tetraethylammonium iron(III) tetrabromide. A constant current of 0.7 $\mu$A was applied for 2−4 weeks at room temperature or 40 °C. Several of the crystal structures of the $\lambda$- and $\kappa$-$(BETS)_2MX_4$ salts (M = Ga, Fe and In; X = Cl and Br) have been reported previously.[9b,11] Figure 1 shows the crystal structure of $\kappa$-$(BETS)_2FeBr_4$ determined at room temperature. One BETS molecule and one-half of the $FeBr_4^-$ anion are crystallographically independent, and the $FeBr_4^-$ anion is on a mirror plane. The molecular structures of BETS radical cation and $FeBr_4^-$ anion with the labeling of the atoms at room temperature are shown in Figure 2 and the BETS molecule has a slightly nonplanar molecular structure. It was found that there is a positional disordering of the carbon C(2) atom of the ethylene group, which is indicated by the higher temperature factor as well as the length of the C(1)−C(2) bond at room temperature. As shown in Figure 1b, the BETS molecules form dimers and adjacent BETS dimers are arranged in a roughly orthogonal manner characteristic of the $\kappa$-type packing motif.[3] There is no essential difference between the already-known molecular arrangements in $\kappa$-$(BETS)_2FeBr_4$ and $\kappa$-$(BETS)_2$-

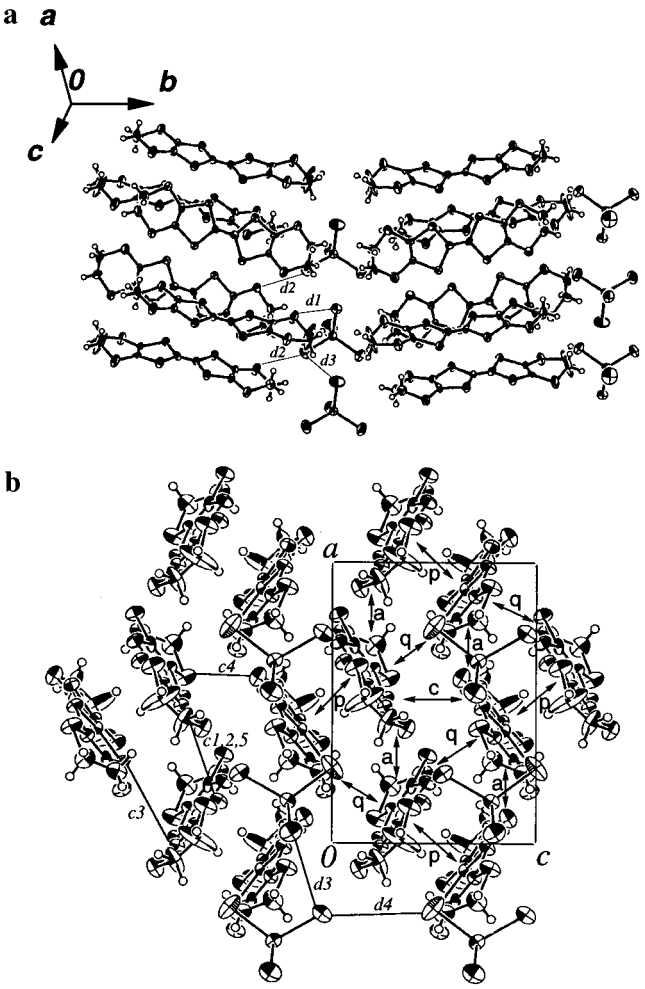


**Figure 1.** (a) Crystal structure of $\kappa$-$(BETS)_2FeBr_4$. (b) Projection along the *b*-axis. The short chalcogen−chalcogen contacts: *c1* [Se(1)−Se(2)] = 3.796(3), *c2* [Se(3)−S(4)] = 3.593(6), *c3* [Se(1)−S(4)] = 3.656(5), *c4* [S(1)−S(3)] = 3.362(8), and *c5* [S(1)−S(2)] = 3.369(8) Å. The short distances: *d1* [Br(3)−S(2)] = 3.693(6), *d2* [Br(1)−S(3)] = 3.708(6), *d3* [Br(1)−Br(3)] = 4.137(4), and *d4* [Br(2)−Br(3)] = 4.637(5) Å. The overlap integrals: *p* 77.33, *a* −22.41, *c* 35.14, and *q* 8.11 × $10^{-3}$.

(7) (a) Day, P.; Kurmoo, M. *J. Mater. Chem.* **1997**, *7*, 1291−1295. (b) Graham, A. W.; Kurmoo, M.; Day, P. *J. Chem. Soc., Chem. Commun.* **1995**, 2061−2062. (c) Kurmoo, M.; Graham, A. W.; Day, P.; Coles, S. J.; Hursthouse, M. B.; Caulfield, J. L.; Singleton, J.; Pratt, F. L.; Hayes, W.; Ducasse, L.; Guionneau, P. *J. Am. Chem. Soc.* **1995**, *117*, 12209−12217. (d) Martin, L.; Turner, S. S.; Day, P.; Mabbs, F. E.; McInnes, E. J. L. *Chem. Commun.* **1997**, 1367−1368.

(8) (a) Clemente-León, M.; Coronado, E.; Galán-Mascarós, J. R.; Gómez-García, C. J.; Rovira, C.; Laukhin, V. N. *Synth. Met.* **1999**, *103*, 2339−2342. (b) Ouahab, L. *Coord. Chem. Rev.* **1998**, *178*−*180*, 1501−1531. (c) Coronado, E.; Gómez-García, C. J. *Chem. Rev.* **1998**, *98*, 273−296.

(9) (a) Kobayashi, H.; Udagawa, T.; Tomita, H.; Bun, K.; Naito, T.; Kobayashi, A. *Chem. Lett.* **1993**, 1559−1562. (b) Kobayashi, H.; Tomita, H.; Naito, T.; Kobayashi, A.; Sasaki, F.; Watanabe, T.; Cassoux, P. *J. Am. Chem. Soc.* **1996**, *118*, 368−377. (c) Akutsu, H.; Arai, E.; Kobayashi, H.; Tanaka, H.; Kobayashi, A.; Cassoux, P. *J. Am. Chem. Soc.* **1997**, *119*, 12681−12682. (d) Sato, A.; Ojima, E.; Kobayashi, H.; Hosokoshi, Y.; Inoue, K.; Kobayashi, A.; Cassoux, P. *Adv. Mater.* **1999**, *11*, 1192−1194. (e) Tanaka, H.; Kobayashi, A.; Sato, A.; Akutsu, H.; Kobayashi, H. *J. Am. Chem. Soc.* **1999**, *121*, 760−768.

(10) (a) Kobayashi, H.; Sato, A.; Arai, E.; Akutsu, H.; Kobayashi, A.; Cassoux, P. *J. Am. Chem. Soc.* **1997**, *119*, 12392−12393. (b) Kobayashi, H.; Sato, A.; Tanaka, H.; Kobayashi, A.; Cassoux, P. *Coord. Chem. Rev.* **1999**, 190−192, 921−932. (c) Sato, A.; Ojima, E.; Akutsu, H.; Kobayashi, H.; Kobayashi, A.; Cassoux, P. *Chem. Lett.* **1998**, 673−674. (d) Kobayashi, H.; Akutsu, H.; Ojima, E.; Sato, A.; Tanaka, H.; Kobayashi, A.; Cassoux, P. *Synth. Met.* **1999**, *103*, 1837−1838.

(11) Kobayashi, A.; Udagawa, T.; Tomita, H.; Naito, T.; Kobayashi, H. *Chem. Lett.* **1993**, 2179−2182.

(12) (a) Tajima, H.; Kobayashi, A.; Naito, T.; Kobayashi, H. *Solid State Commun.* **1996**, *98*, 755−759. (b) Kushch, N.; Dyachenko, O.; Gritsenko, V.; Pesotskii, S.; Lyubovskii, R.; Cassoux, P.; Faulmann, C.; Kovalev, A.; Kartsovnik, M.; Brossard, L.; Kobayashi, H.; Kobayashi, A. *J. Phys. I France* **1996**, *6*, 1997−2009. (c) Harrison, N.; Mielke, C.; Rickel, D.; Montgomery, L.; Gerst, C.; Thompson, J. *Phys. Rev.* **1998**, *B57*, 8751−8754.

(13) Ojima, E.; Fujiwara, H.; Kato, K.; Kobayashi, H.; Tanaka, H.; Kobayashi, A.; Tokumoto, M.; Cassoux, P. *J. Am. Chem. Soc.* **1999**, *121*, 5581−5582.

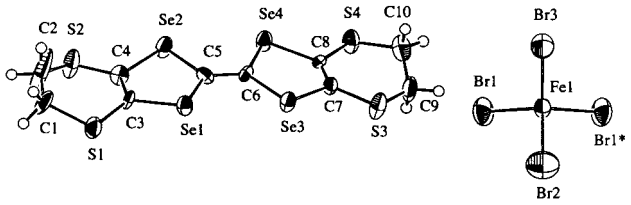


**Figure 2.** Molecular structures of the BETS radical cation and the $FeBr_4^-$ anion with the labeling of the atoms at room temperature.

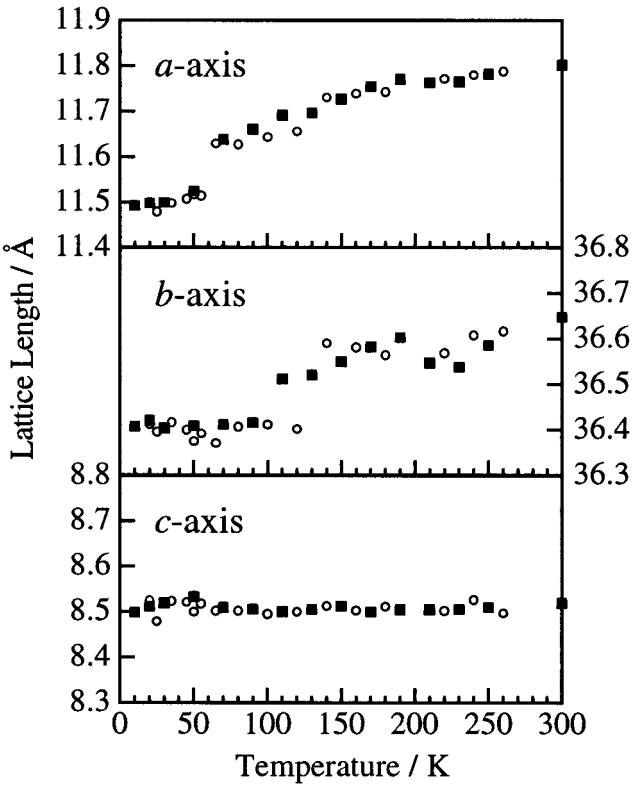


**Figure 3.** Temperature dependence of the lattice constants of $\kappa$-$(BETS)_2FeBr_4$. Filled squares: cooling run. Opened circles: warming run.

$FeCl_4$.[9b,11] The analyses of the BETS intermolecular distances show that there is only one Se−Se type short contact (<3.80 Å), 3.796(3) Å [*c1*: Se(1)−Se(2)], and the shortest Se−S and S−S distances are 3.593(6) [*c2*: Se(3)−S(4)] and 3.362(8) Å [*c4*: S(1)−S(3)], respectively. Two-dimensional conduction layers (the *ac*-plane) composed of the BETS dimers and the insulating layers of the tetrahedral anions with localized magnetic $Fe^{3+}$ moments are arranged alternately along the *b* direction (Figure 1a). In the anion layer, the shortest Fe−Fe distance is 5.921(3) Å along the *a*-axis and 8.504(5) Å along the *c*-axis. Between the $FeBr_4^-$ anion molecules, the shortest Br−Br distance along the *a*-axis is 4.137(4) Å [*d3*: Br(1)−Br(3)], which is much shorter than that along the *c*-axis, 4.637(5) Å [*d4*: Br(2)−Br(3)]; however, these distances are still longer than the sum of the van der Waals radii of bromines (3.7 Å). From these results the direct intermolecular interaction between the $FeBr_4^-$ anion molecules is considered to be weak but relatively stronger along the *a*-axis than along the *c*-axis. There are several short Br−S contacts almost equal to the sum of the van der Waals radii of bromine and sulfur atoms (3.7 Å) between BETS and the anion molecules as indicated in Figure 1a. The shortest Br−S distance is 3.693 (6) Å [*d1*: Br(3)−S(2)]. In the $\lambda$-$(BETS)_2FeCl_4$ salt, the $FeCl_4^-$ anion gets into the donor layer and there is a short Cl−Se contact (3.528 Å) between BETS and the $FeCl_4^-$ anion;[9b] however, no Br−Se contact is observed in the $\kappa$-$(BETS)_2FeBr_4$ salt. Therefore, the interaction between the $\pi$ conduction electrons of the BETS layer and the $Fe^{3+}$ 3d localized spins of the anion molecules in the $\kappa$-$(BETS)_2FeBr_4$ salt is weaker than the case of the $\lambda$-$(BETS)_2FeCl_4$ salt. The temperature dependence of the lattice parameters of $\kappa$-$(BETS)_2FeBr_4$ in the temperature range 270−7 K is shown in Figure 3, where changes of the lattice constants at cooling (filled squares) and warming (opened circles) cycles are presented. Figure 3 displays the presence of some structural anomalies in the temperature range of 60−140 K. Around 100 K, the *b*-parameter shows a hysteresis-like behavior, i.e., there is a decrease of the *b*-parameters for about 0.1 Å between 110 and 90 K at cooling, and practically the same reverse change between 120 and 140 K at warming run. On the other hand, the *a*-parameter of the lattice has a remarkable change at around 60 K both for cooling and for warming cycles. The results of the temperature dependence of lattice constants described above indicate the presence of the structure transformation of $\kappa$-$(BETS)_2FeBr_4$ in the temperature range of 60−140 K. The studies on the crystal structure analyses at low temperatures are now in progress and the details will be reported elsewhere.

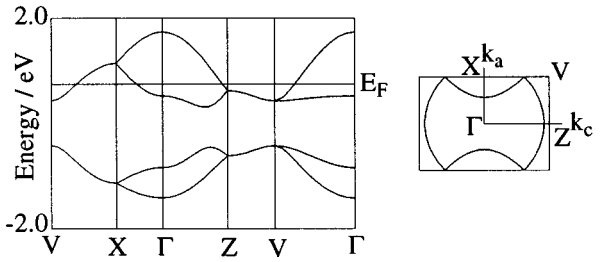


**Figure 4.** Band structure and Fermi surface of $\kappa$-$(BETS)_2FeBr_4$.

**Table 1.** Overlap Integrals, Mid-Gap Energies, and Bandwidths of the Upper Band

| | *a* | *p* | *q* | *c* | *E* mid-gap | bandwidth |
|---|---|---|---|---|---|---|
| $\kappa$-$(BETS)_2FeBr_4$ | −22.41 | 77.33 | 8.11 | 35.14 | 0.68 | 1.44 |
| $\kappa$-$(BETS)_2FeCl_4$[a] | −16.93 | 64.37 | 9.08 | 32.76 | 0.48 | 1.28 |

[a] Taken from ref 9b.

A band dispersion and Fermi surface was calculated on the crystal structure at room temperature based on the extended Hückel approximation as shown in Figure 4. Table 1 shows overlap integrals, mid-gap energies, and the bandwidth of the upper band of the $\kappa$-$(BETS)_2FeBr_4$ salt together with those of the $\kappa$-$(BETS)_2FeCl_4$ salt.[9b] The intradimer overlap integral (*p*, $77.33 \times 10^{-3}$) of the $\kappa$-$(BETS)_2FeBr_4$ salt is much larger than the other overlaps (*a*, −22.41; *q*, 8.11; and *c*, $35.14 \times 10^{-3}$) reflecting the dimer structure of the $\kappa$-type salts. The band dispersion of $\kappa$-$(BETS)_2FeBr_4$ has four energy branches corresponding to the existence of four donor molecules in one unit of the donor sheet. There is a mid-gap between the upper two branches and the lower two branches due to the strong dimerization of the donor molecules as is often observed in $\kappa$-type BEDT-TTF salts and the upper band is effectively half-filled consequently. The energy of the mid-gap of the $\kappa$-$(BETS)_2FeBr_4$ salt is 0.68 eV, which is much larger than that of the $\kappa$-$(BETS)_2FeCl_4$ salt (0.48 eV) corresponding to the strength of the intradimer interaction (*p*), suggesting the stronger electron correlation in the $\kappa$-$(BETS)_2FeBr_4$ salt. The Fermi surface of this salt is a two-dimensional circle closed in the XV boundary as a result of space group symmetry, similar to those of the isostructural $\kappa$-$(BETS)_2FeCl_4$ and $\kappa$-$(BETS)_2GaCl_4$ salts which have been confirmed by the Shubnikov−de Haas

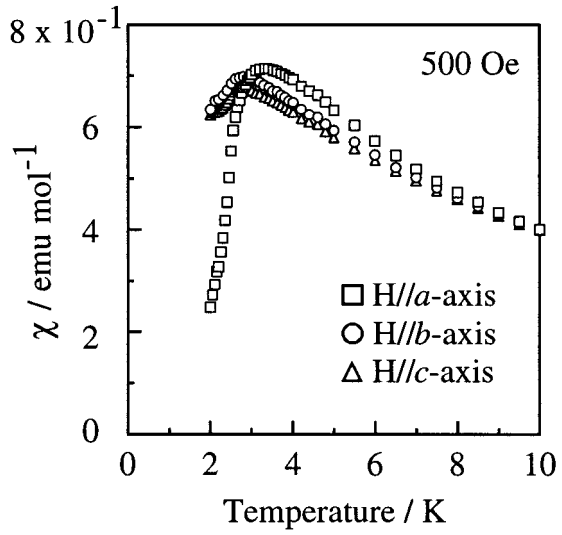


**Figure 5.** Magnetic susceptibility of a platelike single crystal of $\kappa$-$(BETS)_2FeBr_4$ at 500 Oe. $\chi_{//a}$ (opened squares), $\chi_{//b}$ (opened circles), and $\chi_{//c}$ (opened triangles) represent the magnetic susceptibilities for the fields applied to the crystallographic *a*-, *b*-, and *c*-axes, respectively.

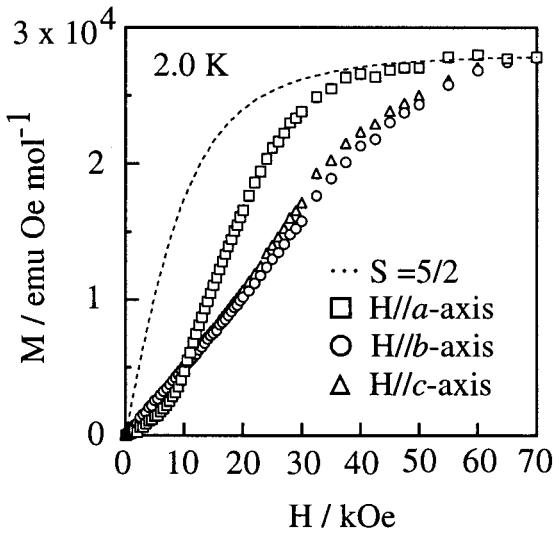


**Figure 6.** Field (H) dependence of the magnetization (M) at 2.0 K of a platelike single crystal of $\kappa$-$(BETS)_2FeBr_4$. The fields were applied along the three axes of crystal lattice. The Brillouin function with $S = {}^5/_2$ is also shown for comparison.

and de Haas−van Alphen oscillations.[9b,12,14] A theoretical study on the effect of the high-spin $Fe^{3+}$ on the two-dimensional electronic system of $\lambda$- and $\kappa$-type BETS salts was made by the calculation with the mean-field approximation for the Coulombic interaction.[15]

**Magnetic Properties of $\kappa$-$(BETS)_2FeBr_4$.** Magnetic susceptibilities were measured on one platelike single crystal (0.22 mg) of $\kappa$-$(BETS)_2FeBr_4$ using a SQUID magnetometer. The measurements were performed by applying magnetic field (500 Oe) along the three crystallographic axes of the single crystal (the *a*-, *b*-, and *c*-axes). The obtained magnetic susceptibilities at 100−300 K can be well fitted by the Curie−Weiss plot, where $\chi T$ is almost constant: $\chi = C/(T - \theta)$, where $C = 4.70$ K emu mol$^{-1}$ and $\theta = -5.5$ K. This negative Weiss temperature ($\theta = -5.5$ K) suggests the dominant magnetic interaction to be antiferromagnetic. The Curie constant ($C = 4.70$ K emu mol$^{-1}$) is approximately equal to 4.38 K emu mol$^{-1}$ [$=N_A g^2 \mu_B S(S + 1)$] expected for the $S = {}^5/_2$ localized spin system with $g = 2.0$. Therefore, the $FeBr_4^-$ anion is cleared to be in the high-spin state.[16] Figure 5 shows the temperature dependence of susceptibilities at 2−10 K. The susceptibilities ($\chi//a$, $\chi//b$, and $\chi//c$) take a maximum around 3 K. Then, a fairly sharp decrease was observed around 2.5 K only when the magnetic field was applied in parallel to the *a*-axis, and $\chi//b$ and $\chi//c$ tend to be constant with lowering temperature. These results indicate the simple antiferromagnetic ordering of $Fe^{3+}$ spins around 2.5 K ($T_N$; Néel temperature) with the easy spin axis parallel to the crystallographic *a*-axis. That is, $\kappa$-$(BETS)_2FeBr_4$ is the first organic conductor with the antiferromagnetic metal phase at ambient pressure. On the other hand, the magnetic field dependence of magnetizations at 2.0 K is shown in Figure 6. A metamagnetic behavior begins to appear from 10 kOe at 2.0 K when the field is applied in parallel with the *a*-axis. The metamagnetic behavior had been observed in a single crystal of $FeCl_2$ and so on.[17] The magnetization (M//*a*) increases rapidly and saturates to the value of the $S = {}^5/_2$ spin system at 30 kOe. When the magnetic field is applied in parallel to the *b*- and *c*-axes, the magnetization increases linearly with increasing external field and tends to be saturated around 60 kOe. However, as shown in Figure 7, no distinct hysteresis of the magnetization (M//*a*) was observed around the spin flipping magnetic field at 2.0 K, though a slight hysteresis behavior seems to exist around 40 kOe where the system is in the forced ferromagnetic state. The metamagnetism suggests the existence of ferromagnetic sublattices coupled antiferromagnetically to each other. The magnitude of the antiferromagnetic interaction between the ferromagnetic sublattices can be estimated from the exchange energy and the

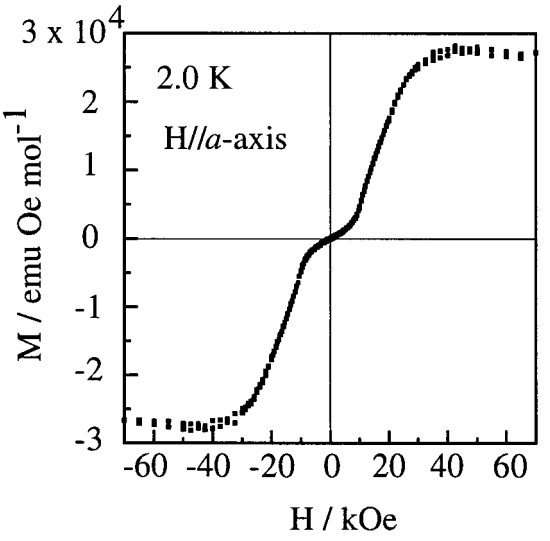


**Figure 7.** Magnetization curve in the measurement cycle between −70 and 70 kOe at 2.0 K.

(14) S. Uji et al. have recently suggested the possibility of the structural change at low temperature because the closed orbits corresponding to about 20% and 100% of the first Brillouin zone were observed in their Shubnikov-de Haas (SdH) oscillation experiments on $\kappa$-$(BETS)_2FeBr_4$ (private communication). It might be possible that the structural change suggested from the low-temperature X-ray diffraction experiments is consistent with the results of SdH experiments. The detailed low-temperature structural studies will be made in the near future.

(15) Hotta, C.; Fukuyama, H. *J. Phys. Soc. Jpn.* **2000** *69*, 2577−2596.

(16) N. Harrison et al. have recently suggested an unusual low-spin state of $Fe^{3+}$ of $\kappa$-$(BETS)_2FeCl_4$ by ESR measurements (ref 12c). But very recently, A. Sato et al. have measured the susceptibility of $\kappa$-$(BETS)_2FeCl_4$ by SQUID magnetometer and confirmed the high spin state of $FeCl_4^-$. The estimated $Fe^{3+}$ spin concentration [per $(BETS)_2FeCl_4$] was 106% by assuming $S = {}^5/_2$ and $g = 2.0$ (ref 9d).

(17) (a) Kanamori, J. *Prog. Theor. Phys.* **1958**, *20*, 890−908. (b) Stryjewski, E.; Giordano, N. *Adv. Phys.* **1977**, *26*, 487−650.

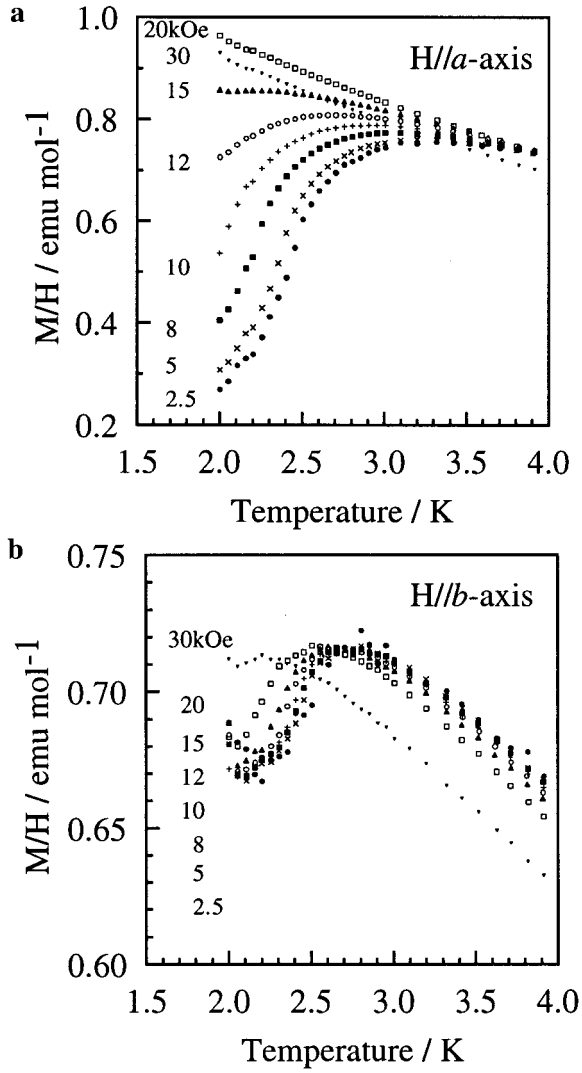


**Figure 8.** Temperature dependence of the magnetic susceptibility of $\kappa$-$(BETS)_2FeBr_4$ at 2.0−4.0 K measured under the indicated magnetic field (a) along the *a*-axis and (b) along the *b*-axis.

magnetic energy at the transition magnetic field $H_c(0)$ at 0 K: $-2z_{AF}J_{AF}S^2 = g\mu_B SH_c(0)$. Here we assume roughly the transition magnetic field $H_c(0) \approx 20$ KOe at 0 K from the line shape of the magnetization curve of Figure 6 (H//*a*-axis) because the curve is not sharp at 2.0 K, and we could obtain the antiferromagnetic exchange of $z_{AF}J_{AF}/k_B = -0.54$ K. According to molecular field theory,[18] the intrasublattice ferromagnetic exchange ($J_F$) and intersublattice antiferromagnetic exchange ($J_{AF}$) are related by the following equation: $(z_FJ_F/z_{AF}J_{AF}) = 3T_Nk_B/(S+1)g\mu_BSH_c(0) - 1$. Adopting the value $z_{AF}J_{AF}/k_B = -0.54$ K and the Néel temperature, $T_N = 2.5$ K, this equation gives us the small ferromagnetic exchange value of $z_FJ_F/k_B = 0.044$ K. Considering the crystal structure of the $\kappa$-$(BETS)_2FeBr_4$ salt, the direct intermolecular interaction between the anions seems to be stronger along the *a*-axis than along the other axes as mentioned before and the interaction through the donor layer will be small in comparison to the others, although we could not neglect it because of the appearance of the three-dimensional antiferromagnetic transition.

Figure 8 shows the temperature dependence of the magnetic susceptibilities under various magnetic fields applied along the *a*- and *b*-axes. When we measured them under the applied magnetic fields along the *c*-axis, the obtained results are almost the same as those of the *b*-axis data. As indicated in Figure 8a, the Néel temperature shifts smoothly to the lower temperatures by the applications of the magnetic fields along the easy-axis (H//*a*) and the antiferromagnetic transition was hardly observed at 20 kOe. On the other hand, when applying the magnetic fields along the hard axes (H//*b* and H//*c*), the shifts of the Néel temperature caused by the magnetic fields are much smaller than those applied along the easy axis and the antiferromagnetic transition almost disappeared at 40 kOe (Figure 8b).

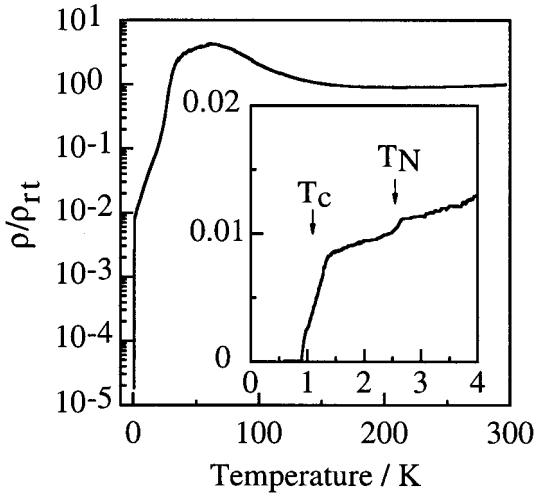


**Figure 9.** Temperature dependence of the electrical resistivity of $\kappa$-$(BETS)_2FeBr_4$ at 0.6−300 K measured along the *ac* plane at zero field. (Inset: in the temperature range between 0.6 and 4.0 K.)

**Electrical Properties of $\kappa$-$(BETS)_2FeBr_4$.** Contrary to the normal metallic behavior of $\kappa$-$(BETS)_2FeCl_4$, $\kappa$-$(BETS)_2FeBr_4$ with the large metal tetrabromide anions shows an anomalous resistivity peak at low temperature.[9b,11] In addition, unlike $\kappa$-$(BETS)_2FeCl_4$ with almost constant resistivity at lowest temperature, $\kappa$-$(BETS)_2FeBr_4$ shows a resistivity decrease with lowering temperature even below 4.2 K. Therefore, the electrical resistivity was measured down to 0.6 K. As shown in Figure 9, the resistivity decreases very slowly down to about 200 K. Then it increases fairly sharply and takes the characteristic peak around 60 K, below which resistivity decreases very rapidly. Such a resistivity peak often has been observed in the $\kappa$-type BEDT-TTF superconducting salts and is considered to be a characteristic behavior for the strong electron correlation system having a strong intradimer interaction. Indeed, the calculation of the intermolecular overlap integrals based on the extended Hückel approximation revealed that the intradimer interaction of the $\kappa$-$(BETS)_2FeBr_4$ salt is stronger than that of the $\kappa$-$(BETS)_2FeCl_4$ salt, which shows no resistivity peak around 60 K. As mentioned before, there are some structural anomalies in the temperature range of 60−140 K (Figure 3). Between 140 and 90 K, the *b*-parameter shows the hysteretic decrease of about 0.1 Å. On the other hand, around 60 K, the *a*-parameter has an abrupt change both for cooling and for warming cycles. It may be possible that the anomaly in the *b*-parameter is related to the conformational change of the terminal ethylene groups of BETS to which the transport properties will be rather insensitive. On the other hand, the anomaly in the *a*-parameter will produce some changes in the electronic band structure. Therefore, this resistivity peak is considered to be associated with not only the strong electron correlation but also some structural transformations.

As seen from the inset of Figure 9, the resistivity shows a small drop at around 2.5 K where the antiferromagnetic transition of the $Fe^{3+}$ spins takes place. This clearly shows that

(18) Jacobs, I. S.; Lawrence, P. E. *Phys. Rev.* **1967**, *164*, 866.

the resistivity is depressed by the onset of the ordering of $Fe^{3+}$ spins and can be regarded as direct evidence for the important role of the interaction between $\pi$ metal electrons and localized magnetic moments. Furthermore, a superconducting transition was observed at 1.1 K. Kobayashi et al. have recently found that the superconducting state of $\lambda$-$(BETS)_2Fe_xGa_{1-x}Br_yCl_{4-y}$ ($0.35 < x < 1$, $y < 0.5$) is broken by the development of antiferromagnetic ordering of $Fe^{3+}$ spins to result in the superconductor-to-insulator or superconductor-to-metal transitions.[10] However, unlike the $\lambda$-$(BETS)_2Fe_xGa_{1-x}Br_yCl_{4-y}$ system, the present study has revealed that $\kappa$-$(BETS)_2FeBr_4$ undergoes the transition from the antiferromagnetic metal phase to the superconducting phase.

As shown in Figure 10a−c, we also measured the resistivities of one platelike crystal along the *a*-axis under the magnetic field applied along the crystallographic three axes, H//*a*, H//*b*, and H//*c* below 5.0 K. When applying the magnetic fields along the easy axis of the antiferromagnetic transition (H//*a*), the resistivity drop at $T_N$ (≈2.5 K) under zero magnetic field shifts quickly to the lower temperatures and disappears at 18 kOe. On the other hand, when we applied the magnetic fields along the *b*- and *c*-axes (the hard-axes), the temperature shifts of the resistivity drop are very small up to 10 kOe and then the drop gradually moves to the lower temperatures and vanishes at 40 kOe. As Figure 11 indicates, the magnetic field dependence of the temperature of the resistivity drops is completely the same as that of the Néel temperatures ($T_N$) measured by the SQUID magnetometer. Furthermore, the magnetic fields where the resistivity drop could not be observed at all are almost the same as the fields where the decrease of the magnetic susceptibility was not detected. These results undoubtedly prove that the resistivity drops at the Néel temperature have originated from the antiferromagnetic ordering of the $Fe^{3+}$ localized spins and there is certainly $\pi$−d interaction between the BETS $\pi$-conduction electron system and the $Fe^{3+}$ d-spin system. Furthermore, the temperature dependence of the resistivities is still metallic under the applied magnetic field over 30 kOe along the *a*-axis. It is clear that the metallic state coexists with the forced ferromagnetic state metamagnetically induced by the applied magnetic field.

We defined the superconducting transition temperature $T_c$ where the resistivities decrease to 50% of the normal metallic state value at 1.3 K. A sharp superconducting transition is observed at 1.1 K under zero magnetic field with the transition temperature width of 0.6 K and is suppressed by the application of the magnetic field. However, the suppression of the superconducting transition varies remarkably from the direction of the applied magnetic fields. As shown in Figure 10b, when the magnetic field was applied perpendicular to the conduction *ac*-plane (H//*b*), the superconducting state was quickly broken and normal metallic state was recovered at an weak magnetic field over 2 kOe. This is in consistent with the cases of the $\kappa$-type two-dimensional organic superconductors such as the $\kappa$-$(BEDT\text{-}TTF)_2X$ salts,[4,19] in which the superconducting state is quite anisotropic and the upper critical field when the field is applied perpendicular to the conduction plane is considerably smaller than is the case when the field is applied parallel to the conduction plane. However, the superconducting state of the

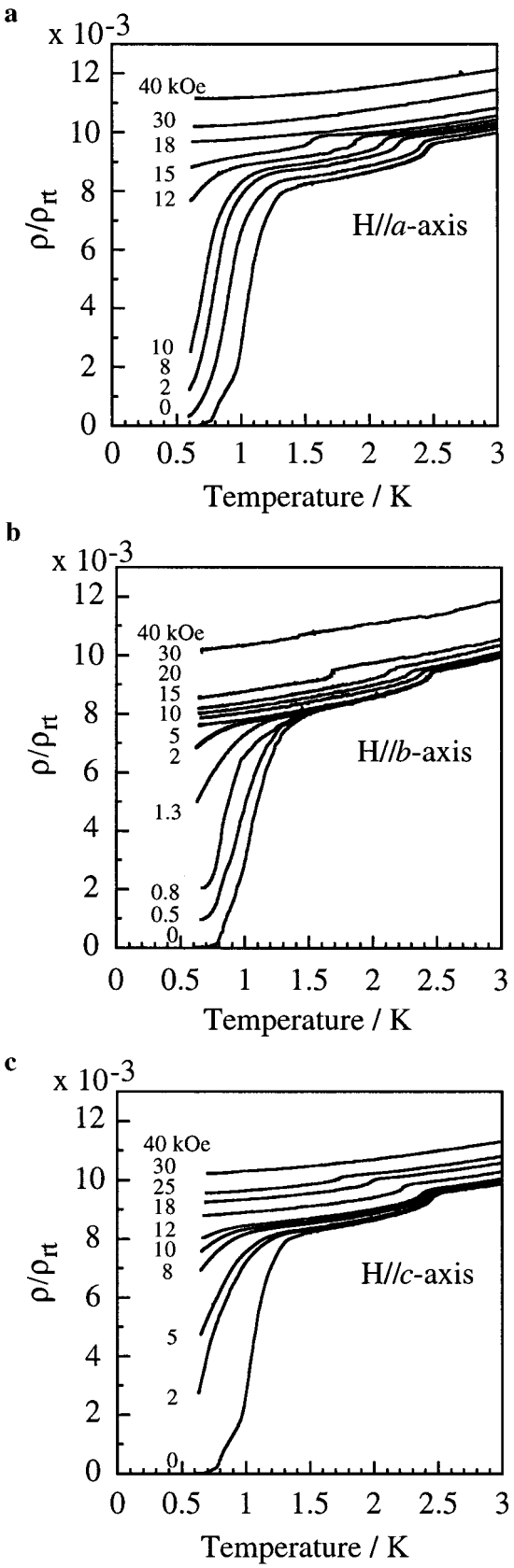


**Figure 10.** Temperature dependence of the electrical resistivity of $\kappa$-$(BETS)_2FeBr_4$ at 0.6−3.0 K measured along the *a*-axis under the indicated magnetic field (a) along the *a*-axis, (b) along the *b*-axis, and (c) along the *c*-axis.

(19) (a) Oshima, K.; Urayama, H.; Yamochi, H.; Saito, G. *J. Phys. Soc. Jpn.* **1988**, *57*, 730−733. (b) Murata, K.; Honda, Y.; Anzai, H.; Tokumoto, M.; Takahashi, K.; Kinoshita, N.; Ishiguro, T.; Toyota, N.; Sasaki, T.; Muto, Y. *Synth. Met.* **1988**, *27*, A341−A346. (c) Kwok, W. K.; Welp, U.; Carlson, K. D.; Crabtree, G. W.; Vandervoort, K. G.; Wang, H. H.; Kini, A. M.; Williams, J. M.; Stupka, D. L.; Montgomery, L. K.; Thompson, J. E. *Phys. Rev.* **1990**, *B42*, 8686−8689. (d) Nakamura, T.; Komatsu, T.; Saito, G.; Osada, T.; Kagoshima, S.; Miura, N.; Kato, K.; Maruyama, Y.; Oshima, K. *J. Phys. Soc. Jpn.* **1993**, *62*, 4373−4385. (e) Wosnitza, J.; Wanka, S.; Beckmann, D.; Hagel, J.; Balthes, E.; Schweitzer, D.; Strung, W.; Keller, H. *Synth. Met.* **1997**, *85*, 1557−1558.

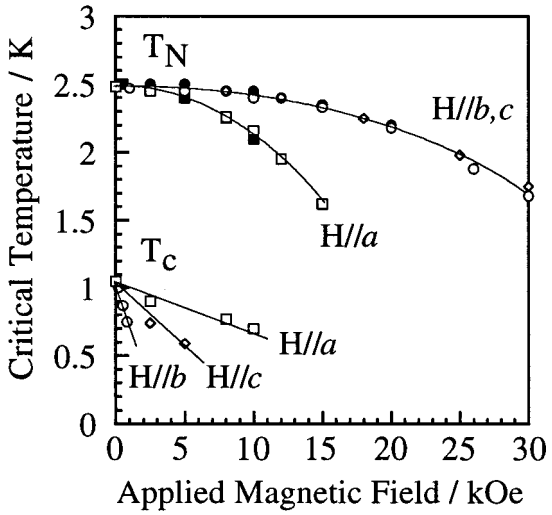


**Figure 11.** The H−T plots of the Néel temperatures ($T_N$) and the superconducting transition temperatures ($T_c$) under the magnetic fields applied along the three axes (squares, *a*-axis; circles, *b*-axis; and triangles, *c*-axis) determined by electrical resistivity measurements (opened symbols) and SQUID measurements (closed symbols).

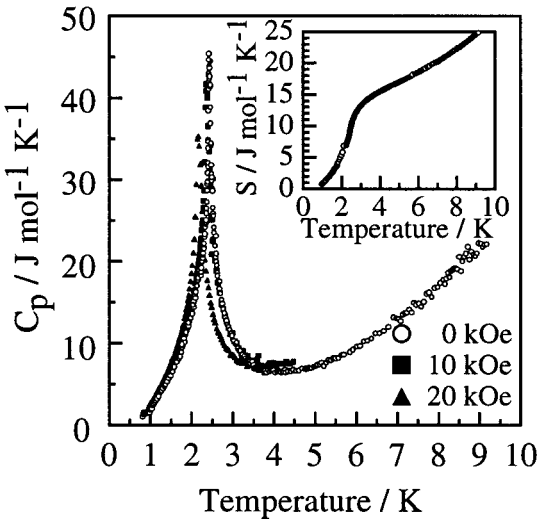


**Figure 12.** The temperature dependence of zero-field specific heat of $\kappa$-$(BETS)_2FeBr_4$ at 0.9−9 K. (Inset: The temperature dependence of entropy distribution around the peak.)

conventional $\kappa$-type salt is usually almost isotropic in the conduction plane. In the $\kappa$-$(BETS)_2FeBr_4$ salt, on the other hand, the situation is quite complex due to the existence of the antiferromagnetic ordering and metamagnetic behavior of the $Fe^{3+}$ localized internal spin system. When applying the magnetic field along the easy axis of the antiferromagnetic transition (H//*a*), the superconducting transition was slowly suppressed up to 10 kOe, then suddenly almost broken at 12 kOe. On the other hand, the application of the magnetic field along the hard axis (H//*c*) made a quicker suppression of the superconducting state than is the case when the field is applied along the easy axis. The superconducting critical temperatures were determined from the resistivity measurements shown in Figure 10a−c and are also plotted in the $H-T$ phase diagram (Figure 11). The $T_c$ decreases almost linearly to the applied magnetic field below $T_c$ with slopes of $dT_c/dH//a = -0.04$, $dT_c/dH//b = -0.44$, and $dT_c/dH//c = -0.11$ K/kOe. As mentioned before, when the magnetic field was applied along the easy axis, the magnetization of the $Fe^{3+}$ spins is very small under a field lower than the critical field of the metamagnetic transition because of the antiferromagnetic ordering of the $Fe^{3+}$ spins. On the other hand, the magnetization under the magnetic field applied along the hard axis increases linearly with increasing outer magnetic field. Therefore, we conclude that the intraplane anisotropic behavior of the magnetic field dependence of the superconducting state originates from the difference of the internal magnetic field produced by the magnetization of the $Fe^{3+}$ d-spins of the anion layers, which is anisotropically induced by the outer magnetic field.

**Temperature Dependence of the Specific Heat of $\kappa$-$(BETS)_2FeBr_4$.** In the $\lambda$-$(BETS)_2Fe_xGa_{1-x}Br_yCl_{4-y}$ ($0.35 < x < 1$, $y < 0.5$) system, the superconducting state is broken by the development of antiferromagnetic ordering of $Fe^{3+}$ spins because of the strong coupling between $\pi$ and d electron systems.[10] On the other hand, the $\kappa$-$(BETS)_2FeBr_4$ salt shows the transition from the antiferromagnetic metal phase to the superconducting phase. It is of considerable interest to study whether the antiferromagnetic spin ordering and superconductivity coexist below the Néel temperature. To confirm the bulk nature of the phase transitions and to inquire into the possibility of the coexistence of spin ordering and superconductivity at low temperatures, specific heat measurements were performed by the thermal relaxation method using a $^3He$ cryostat down to about 0.9 K. Several pieces of thin platelike crystals of which the total weight is 0.19 mg were attached on the sample holder by a small amount of Apiezon N grease. The heat capacity of the sample holder including the grease is subtracted from the total heat capacity and the Cp vs *T* curve for the present crystals is shown by open circles in Figure 12. To confirm the absolute precision of the data, the measurement below 2.7 K was reproduced for two pieces of sample (total weigh 0.12 mg) and also plotted by the opened circles in the same figure. From Figure 12, it is clear that the zero-field specific heat shows a large anomaly characterized by a sharp $\lambda$-type peak at about 2.4 K, which corresponds to the antiferromagnetic transition temperature detected by the magnetic susceptibility and resistivity measurements. The integration of the Cp/*T* vs *T* curve with respect to temperature gives the information on the entropy [*S*(*T*)] distribution around the peak, which is shown in the inset of Figure 12. Although we cannot exclude the additional entropy coming from the lattice specific heat that becomes gradually larger with increasing temperature, the value of the entropy [*S*(*T*)] reaches $R \ln 6$ ($=R \ln(2S + 1) = 14.9$ J mol$^{-1}$ K$^{-1}$), corresponding to the full entropy coming from the magnetic specific heat based on the degenerate freedom of $S = 5/2$ spins, at about 3.8 K. By applying magnetic fields perpendicular to the *ac*-plane, the peak position shifts to lower temperatures of 2.36 K at 10 kOe and 2.05 K at 20 kOe, respectively, and these temperatures almost correspond to those obtained from the measurement of the magnetic susceptibilities and the electrical resistivities. These results imply that the magnetic order is surely an antiferromagnetic one and the spin state is the $S = 5/2$ high-spin state of trivalent iron ions ($Fe^{3+}$). In addition to this, we cannot detect any anomaly around the superconducting transition temperature (1.1 K), which demonstrates that the magnetically ordered state is not destroyed by the appearance of another phase transition, namely the superconducting transition in the $\pi$-electron layers. Therefore, it is possible to assert that the magnetic order and the superconductivity coexist at low temperatures below $T_c = 1.1$ K. This is the first organic salt in which the long-range magnetic ordering of the magnetic anions mediated by $\pi$-donor molecules and the superconductivity based on the $\pi$-electrons in the donor layers coexist in the hybrid structure composed of the antiferromagnetic insulator and superconductor

layers. In the inorganic materials, the coexistence of the antiferromagnetic state and superconductivity had been observed in the ternary systems such as the rhodium−boride phase, $RERh_4B_4$ (RE = Nd, Sm), and the so-called Chevrel compounds, $REMo_6S_8$ (RE = Gd, Tb, Dy, and Er), in which the 4d electrons of Rh or Mo atoms show superconductivity and the 4f spins of rare earth atoms antiferromagnetically order below the superconducting transition temperature.[20,21] However, the phase transition from the antiferromagnetic metal phase to the antiferromagnetic superconducting phase as is observed in the $\kappa$-$(BETS)_2FeBr_4$ salt is quite unusual and only one system, $Ho(Ir_xRh_{1-x})_4B_4$ ($x \geq 0.6$), was reported to our knowledge.[22]

## Conclusion

The electrical and magnetic properties of $\kappa$-$(BETS)_2FeBr_4$ show this system to be the first antiferromagnetic organic metal at ambient pressure ($T_N$ = 2.5 K). The characteristic field dependence of the magnetization at 2.0 K and the temperature dependence of susceptibilities indicates the antiferromagnetic spin structure with the easy axis parallel to the *a*-axis. When the magnetic field is applied in parallel with the *a*-axis, the magnetization increases very rapidly from 10 kOe and tends to be saturated around 30 kOe, indicating the metamagnetic behavior. On the other hand, the magnetization increases almost linearly up to about 60 kOe for the field parallel to the *b*- and *c*-axis. The small resistivity drop observed at $T_N$ clearly shows the existence of the interaction between $\pi$ metal electrons and localized magnetic moments. In addition, this system undergoes a superconducting transition at about 1.1 K. That is, $\kappa$-$(BETS)_2FeBr_4$ is the first antiferromagnetic organic metal exhibiting a superconducting transition below Néel temperature. We measured the magnetic field dependence of the superconducting critical temperatures in all three crystallographic axes. These results indicated that the superconductivity in this system is strongly anisotropic also in the conduction plane because of the existence of the metamagnetically induced internal field based on the antiferromagnetic ordering of the $Fe^{3+}$ d-spins in contrast to the cases of the other conventional organic superconductors. Therefore this salt is the first $\pi$−d interacting organic superconductor in which the superconducting state is affected by the internal d-spin system. We also observed the $\lambda$-type large peak of zero-field specific heat corresponding to the three-dimensional antiferromagnetic transition of the high-spin $Fe^{3+}$ ion. From the thermodynamic properties for the low-temperature region below $T_N$, the possibility of the coexistence of superconductivity and magnetic order is strongly indicated. Some peculiar resistive and magnetic properties under magnetic fields related to vortex dynamics are expected to occur in this system which may be an interesting future problem.

## Experimental Section

**General.** Bis(ethylenedithio)tetraselenafulvalene (BETS) was synthesized as described in the literature.[23] The supporting electrolyte, tetraethylammonium iron(III) tetrabromide, was prepared by the reaction of tetraethylammonium bromide and iron(III) tribromide in hot ethanol, recrystallized several times from acetone−ethanol solution, and dried in vacuo. Chlorobenzene (PhCl) was washed three times with concentrated sulfuric acid, then with aqueous sodium hydrogen carbonate solution and water, followed by drying with calcium chloride, and distilled over diphosphorus pentaoxide under nitrogen atmosphere. Ethanol (EtOH) was distilled over magnesium ethoxide under nitrogen and stored in a refrigerator until use.

**Preparation of $\kappa$-$(BETS)_2FeBr_4$.** The single crystals of $\kappa$-$(BETS)_2FeBr_4$ were prepared electrochemically. BETS (6.5 mg) and tetraethylammonium iron(III) tetrabromide (57 mg) were dissolved in 10% ethanol/chlorobenzene solution (15.0 mL) under nitrogen. After several days, constant current (0.7 $\mu$A) was applied between the electrodes at room temperature or at 40 °C for 2−4 weeks. Thin plate-shaped crystals of $\kappa$-type salt were obtained.

**Crystallographic Data Collection and Structure Determination.** Room temperature data collection for the plate-shaped crystal (dimensions 0.25 × 0.20 × 0.01 $mm^3$) of $\kappa$-$(BETS)_2FeBr_4$ was performed on a Rigaku AFC-5R diffractometer with graphite monochromated Mo K$\alpha$ radiation ($\lambda$ = 0.71069 Å) and a rotating anode generator. Crystal data: $C_{10}H_8S_4Se_4Fe_{0.5}Br_2$, $M$ = 759.98, orthorhombic, space group *Pnma* (no. 62), $a$ = 11.787(6) Å, $b$ = 36.607(9) Å, $c$ = 8.504(5) Å, $V$ = 3669(2) $Å^3$, $Z$ = 8, $\rho_{calcd}$ = 2.751 g $cm^{-3}$, $\mu$ = 131.90 $cm^{-1}$, $F(000)$ = 2808.00. Cell constants were determined from 23 carefully centered reflections in the range $22.4 < 2\theta < 24.8°$. Intensity data were collected to a maximum $2\theta$ value of 60.0° by the $\omega-2\theta$ scan technique with a scan speed of 4.0 deg $min^{-1}$. The number of collected reflections was 6011. An empirical absorption correction based on azimuthal scans of several reflections was applied which resulted in transmission factors ranging from 0.2595 to 1.0000. The data were corrected for Lorentz and polarization effects. The structure was solved by direct method (SHELXS86).[24] The atomic scattering factors were taken from the *International Table for X-ray Crystallography*.[25] The non-hydrogen atoms were anisotropically refined by the full-matrix least-squares method. Hydrogen atoms were included but not refined. The final cycle of full-matrix least-squares refinement was based on 1485 observed reflections [$I > 3.0\sigma(I)$] and 190 variable parameters against $|F|$. $R$ = 0.053, $Rw$ = 0.049, GOF = 1.42. All calculations were performed using the teXsan crystallographic software package of Molecular Structure Corporation.[26]

The measurements of the lattice parameters at low temperatures were performed by using a Mac Science Imaging Plate system (a rotating anode, Mo K$\alpha$) equipped with a closed-cycle helium-cooling device. To determine the lattice parameters two sets of oscillation and Weissenberg type patterns taken on two positions at an interval of 90° were used.

**Band Structure Calculations.** The transfer integrals, band structure, and Fermi surface were calculated by a tight-binding method based on the extended Hückel approximation.[27] Slater-type atomic orbitals were used for the calculation of molecular orbitals. The parameters of the atomic orbitals are the same as those used in $\lambda$- and $\kappa$-$(BETS)_2FeCl_4$ salts (ref 9b). The exponent $\zeta$ and the ionization potential (eV) are the following: Se 4s, 2.112, −20.0; Se 4p, 1.827, −11.0; Se 4d, 1.500, −6.8; S 3s, 2.122, −20.0; S 3p, 1.827, −11.0; S 3d, 1.500, −5.4; C 2s, 1.625, −21.4; 2p, 1.625, −11.4; and H 1s, 1.0, −13.6.

**Electrical Resistivity Measurement.** The ac resistivity was measured down to 0.60 K with a four-probe technique on a Huso Electro Chemical System HECS 994C-1 Multichannel 4-terminal conductometer. Electrical contacts were achieved with gold paste and gold wire (10 $\mu$m $\phi$). Cooling of samples down to 1.5 K was performed by means of pumping liquid $^4$He, and the experiments below 1.5 K were performed by means of pumping liquid $^3$He. Cerenox thermometer was used down to 0.60 K.

(20) (a) Matthias, B. T.; Corenzwit, E.; Vandenberg, J. M.; Barz, H. E. *Proc. Natl. Acad. Sci. U.S.A.* **1977**, *74*, 1334−1335. (b) Vandenberg, J. M.; Matthias, B. T. *Proc. Natl. Acad. Sci. U.S.A.* **1977**, *74*, 1336−1337. (c) Matsumoto, H.; Umezawa, H. *Cryogenics* **1983**, 37−51.

(21) (a) Chevrel, R.; Sergent, M.; Prigent, J. *J. Solid State Chem.* **1971**, *3*, 515−519. (b) Fischer, Ø. *Appl. Phys.* **1978**, *16*, 1−28. (c) Ishikawa, M.; Fischer, Ø.; Muller, J. *J. Phys.* **1978**, *C6*, 1379−1384. (d) Fischer, Ø.; Ishikawa, M.; Pelizzone, M.; Treyvaud, A. *J. Phys.* **1979**, *C5*, 89−94.

(22) Ku, H. C.; Acker, F.; Matthias, B. T. *Phys. Lett.* **1980**, *76A*, 399−402.

(23) Kato, R.; Kobayashi, H.; Kobayashi, A. *Synth. Met.* **1991**, *41-43*, 2093−2096.

(24) SHELXS86: Sheldrick, G. M. In *Crystallographic Computing 3*; Sheldrick, G. M., Kruger, C.,Goddard, R., Eds.; Oxford University Press, 1985; p 175.

(25) Cromer, D. T.; Waber, J. T. In *International Tables for X-ray Crystallography*; Kynoch Press: Birmingham, England, 1974; Vol. 4, Table 2.2A.

(26) teXsan: Crystal Structure Analysis Package, Molecular Structure Corporation, 1985 and 1992.

(27) Hoffmann, R. *J. Chem. Soc., Chem. Commun.* **1963**, *39*, 1397.

**Static Magnetic Susceptibility Measurement.** Measurement of magnetic susceptibility was carried out using a Quantum Design MPMS-7 SQUID magnetometer in a temperature range from 300 to 2.0 K. The field dependence of the magnetization ($M-H$ curve) was measured at 2.0 K up to 70 kOe and down to −70 kOe. All the measurements used a transparency sheet folded into a box and Apiezon M grease. One single crystal (0.22 mg) was fixed on one inner surface of the box with Apiezon M grease. The magnetic fields were applied to the three crystallographic axes (the *a*-, *b*-, and *c*-axes) of the crystal by a manual rotation of the transparency. The same measurement was carried out on the transparency and the grease without the sample. The data were corrected for the diamagnetic contribution estimated from Pascal's constants.

**Specific Heat Measurement.** Specific heat was measured by the thermal relaxation method using a $^3$He cryostat down to about 0.9 K. Several pieces of thin platelike crystals of which the total weight is 0.19 mg were attached on the sample holder by a small amount of Apiezon N grease. The heat capacity of the sample holder including the grease was subtracted from the total heat capacity.

**Acknowledgment.** This work is financially supported by a Grant-in-Aid for Scientific Research on Priority Areas (B) of Molecular Conductors and Magnets (Nos. 11224101 and 11224211) from the Ministry of Education, Science, Sports and Culture, Japan.

**Supporting Information Available:** An X-ray crystallographic file (CIF) . This material is available free of charge via the Internet at http://pubs.acs.org.

JA002439X